ADVANCED HEALTHCARE MATERIALS
www.advhealthmat.de

# Dendritic Polyglycerol-Conjugated Gold Nanostars for Metabolism Inhibition and Targeted Photothermal Therapy in Breast Cancer Stem Cells

*Yuanwei Pan, Suqiong Zhou, Chuang Liu, Xuehua Ma, Jie Xing, Badri Parshad, Wenzhong Li,* Aiguo Wu,* and Rainer Haag**

**Breast cancer stem cells (CSCs) are believed to be responsible for tumor initiation, invasion, metastasis, and recurrence, which lead to treatment failure. Thus, developing effective CSC-targeted therapeutic strategies is crucial for enhancing therapeutic efficacy. In this work, GNSs-dPG-3BP, TPP, and HA nanocomposite particles are developed by simultaneously conjugating hexokinase 2 (HK2) inhibitor 3-bromopyruvate (3BP), mitochondrial targeting molecule triphenyl phosphonium (TPP), and CSCs targeting agent hyaluronic acid (HA) onto gold nanostars-dendritic polyglycerol (GNSs-dPG) nanoplatforms for efficient eradication of CSCs. The nanocomposite particles possess good biocompatibility and exhibit superior mitochondrial-bound HK2 binding ability via 3BP to inhibit metabolism, and further induce cellular apoptosis by releasing the cytochrome c. Therefore, it enhanced the therapeutic efficacy of CSCs-specific targeted photothermal therapy (PTT), and achieved a synergistic effect for the eradication of breast CSCs. After administration of the synergistic treatment, the self-renewal of breast CSCs and the stemness gene expression are suppressed, CSC-driven mammosphere formation is diminished, the in vivo tumor growth is effectively inhibited, and CSCs are eradicated. Altogether, GNSs-dPG-3BP, TPP, and HA nanocomposite particles have been developed, which will provide a novel strategy for precise and highly efficient targeted eradication of CSCs.**

## 1. Introduction

Breast cancer stem cells (CSCs) have the capacity to undergo infinite proliferation and differentiation into multiple cancer cell types, which are highly tumorigenic and believed to be causative for tumor initiation, invasion, metastasis, and recurrence.[1–3] Accumulating evidence proposed that CSCs stemness properties are closely related to metabolism modulation.[4] Therefore, inhibiting the CSCs' metabolism is a promising therapeutic strategy.[5,6] Glycolysis is the primary metabolism form of cancer cells, which is known as the Warburg effect,[7] and recent studies found that breast CSCs exhibit distinctive metabolic features, particularly a higher rate of glycolysis compared to cancer cells.[8,9] The first step of the glycolysis is converting glucose to form glucose-6-phosphate via transferring a phosphate group from adenosine triphosphate (ATP) to glucose, in which hexokinase 2 (HK2) is a key glycolytic enzyme involved in the transfer.[10] Moreover, HK2 bound to the outer mitochondrial membrane by interacting with voltage-dependent anion channel (VDAC), thereby the mitochondrial-bound HK2 could acquire the adjacent ATP and consequently accelerate the glycolytic rate.[11] In addition, the interactions between HK2 and VDAC would also cause resistance to apoptosis by closing the mitochondrial permeability transition pores and suppressing cytochrome c release.[12] The important roles for integrating glycolysis promotion and apoptosis inhibition make the HK2 an attractive target for inhibiting CSCs metabolism.

3-bromopyruvate (3BP) has been presented as a potent HK2 inhibitor, which can be used to suppress the glycolytic capacity of CSCs.[13–15] However, owing to the non-specific properties of 3BP and special defense mechanisms of CSCs, the CSCs metabolism inhibition therapeutic efficacy of 3BP is limited. One potential strategy to overcome these drawbacks is synergistic therapy.[16–19] Nanomaterial-mediated photothermal therapy (PTT) is a promising approach for CSCs synergistic therapy, which utilizes the high temperature to ablate CSCs.[20] The advantage of PTT is minimally invasive, and highly localized ablation with minimal

Y. Pan, S. Zhou, B. Parshad, W. Li, R. Haag
Institute of Chemistry and Biochemistry
Freie Universität Berlin
Takustrasse 3, Berlin 14195, Germany
E-mail: wenzhong.li@fu-berlin.de; haag@chemie.fu-berlin.de
C. Liu, X. Ma, J. Xing, A. Wu
Cixi Institute of Biomedical Engineering
CAS Key Laboratory of Magnetic Materials and Devices, & Key Laboratory of Additive Manufacturing Materials of Zhejiang Province
Ningbo Institute of Materials Technology and Engineering
Chinese Academy of Sciences
Ningbo 315201, P. R. China
E-mail: aiguo@nimte.ac.cn

The ORCID identification number(s) for the author(s) of this article can be found under https://doi.org/10.1002/adhm.202102272



**DOI: 10.1002/adhm.202102272**

damage to normal tissue.[21] Various gold nanomaterials for PTT have been reported, such as gold nanorods, gold nanoshells, and gold nanocages.[22] Unlike their complex synthesis and the potential toxicity from substrates such as cetyltrimethylammonium bromide (CTAB), the synthesis of gold nanostars (GNSs) is simple and CTAB-free. Furthermore, GNSs exhibit a high absorption-to-scattering ratio in the NIR region, making them ideal for an efficient PTT transducer.[23] Moreover, their localized surface plasmon resonance (LSPR) in the near-infrared (NIR) region matches the transparent window from 700 to 900 nm, which could penetrate deeply into tumor tissues, especially the CSCs located inside the tumor.[24,25] We therefore want to explore GNSs-mediated PTT along with CSCs metabolism inhibition to kill CSCs.

The therapeutic efficacy of the synergistic nanoplatform is largely determined by the selective targeting ability to the CSCs in tumor.[26,27] It should be noted that, the majority of HK2 was mainly bound to mitochondria, therefore mitochondrial targeting achieved by triphenyl phosphonium (TPP) could improve the binding ability with HK2 and enhance the metabolism inhibition efficiency of 3BP.[28–30] In addition, inhibition of mitochondrial-bound HK2 led to the mitochondrial permeability increase and subsequent release of cytochrome c to induce the cellular apoptosis after the therapy.[31] Furthermore, functionalization of the nanoplatform with hyaluronic acid (HA) for targeting the breast CSCs is also an effective strategy, in which the HA can specifically bind to cell surface marker CD44 that is overexpressed on breast CSCs.[32] To improve the biocompatibility and obtain a long blood circulation of the nanoplatform, dendritic polyglycerol (dPG) is used. Our previous work has proven that the biocompatibility of nanoparticles is significantly improved after modification with dPG.[33–37] Moreover, the highly branched structure surface and multiple attachment sites of dPG can also facilitate the attachment of 3BP, TPP, and HA.[38] Therefore, based on the GNSs-dPG nanoplatform conjugated with 3BP, TPP, and HA, the synergistic metabolism inhibition and CSCs specific-targeted PTT could be achieved.

In the present study, we developed GNSs-dPG-3BP, TPP, and HA nanocomposite particles by simultaneous conjugation of HK2 inhibitor 3BP, the mitochondrial targeting molecule TPP, and CSCs targeting agent HA onto GNSs-dPG nanoplatform for combined metabolism inhibition and CSCs-specific targeted PTT. The designed GNSs-dPG-3BP, TPP, HA nanocomposite particles possess excellent biocompatibility, superior binding ability with mitochondrial-bound HK2, effective CSCs-specific targeted capability, and excellent photothermal performance under NIR laser irradiation. Moreover, the nanocomposite particles could suppress the metabolism by inhibiting mitochondrial-bound HK2 via 3BP and simultaneously enhancing the therapeutic efficacy of PTT in breast CSCs by inducing cellular apoptosis through the release of the cytochrome c. Our results demonstrated that the GNSs-dPG-3BP, TPP, and HA nanocomposite particles can be utilized to effectively eliminate the CSCs, achieving simultaneous synergistic metabolism inhibition and CSCs-specific targeted PTT, and offering a tremendous potential for precise and highly efficient elimination of CSCs.

## 2. Results and Discussion

The synthesis of GNSs-dPG-3BP, TPP, and HA nanocomposite particles is shown in **Figure 1**. The GNSs were prepared by a reported surfactant-free, seed-mediated growth method. Subsequently, thiolated dPG-3BP, dPG-TPP, and dPG-HA were modified onto the surface of GNSs respectively to obtain GNSs-dPG-3BP, TPP, and HA via Au-S bonds. The dPG rendered GNSs excellent biocompatibility, the conjugated 3BP and TPP could be used for suppressing the metabolism by inhibiting mitochondrial-bound HK2, and the HA was used for targeting CSCs via CD44 overexpressed on breast CSCs. Thus, the prepared GNSs-dPG-3BP, TPP, and HA nanocomposite particles could be applied to eradicate CSCs by suppressing the metabolism and CSCs-specific targeted PTT for the inhibition of tumor growth.

### 2.1. Synthesis and Characterization of GNSs-dPG-3BP, TPP, HA Nanocomposite Particles

The obtained GNSs were observed by TEM. The TEM images of GNSs nanoparticles were well displayed the multi-branched morphologies, which have a mean diameter of about 40 nm (**Figure 2**a). The hydrodynamic size of various nanocomposite particles was characterized by DLS. As shown in Figure 2b, the size of the GNSs was about 47.6 nm, which suggested excellent dispersibility. The hydrodynamic diameter was observed to be slightly larger than the TEM imaging due to the interference of the dispersant into the hydrodynamic diameter. The size of GNSs-dPG, GNSs-dPG-3BP, GNSs-dPG-3BP, TPP, and GNSs-dPG-3BP, TPP, HA were 56.5 nm, 64.2nm, 70.0 nm, and 74.2 nm, respectively. The increased radius was attributed to the surface modification on the GNSs. The UV-vis spectra of various nanocomposite particles were recorded by UV−vis spectrometer (Figure 2c). The broad plasmon resonance absorption bands of GNSs were from 500 to 1100 nm and peak at 800 nm. The various nanocomposite particles that had shown similar plasmon spectra indicated that each step of modification would not change the plasmon spectra and without severe aggregation. The Fourier transform infrared (FTIR) measurements further confirmed the successful functionalization of dPG on the surface of GNSs (Figure S1, Supporting Information) After coupling with the dPG, the O−H alcoholic stretching (3500−3100 $cm^{-1}$), aliphatic C−H stretching (3000−2850 $cm^{-1}$), and C−O−C ether stretching (1150−1000 $cm^{-1}$) spectra were recorded as characteristic signals of dPG scaffold. The bands located at 1650−1550 $cm^{-1}$ corresponding to N−H stretching indicated the presence of amino groups.

Photothermal performance plays important role in the PTT therapeutic application. The GNSs have been reported as a superior photothermal agent and exhibited excellent photothermal efficacy owing to their multiple sharp branches and strong SPR properties.[23] The photothermal performance of bare GNSs and various GNSs nanocomposite particles was investigated by IR thermal imaging system and an 808 nm laser. As shown in Figure 2d, the GNSs were exposed to 808 nm laser at 1.5 W $cm^{-2}$, the temperature could obviously increase from 24.0 to

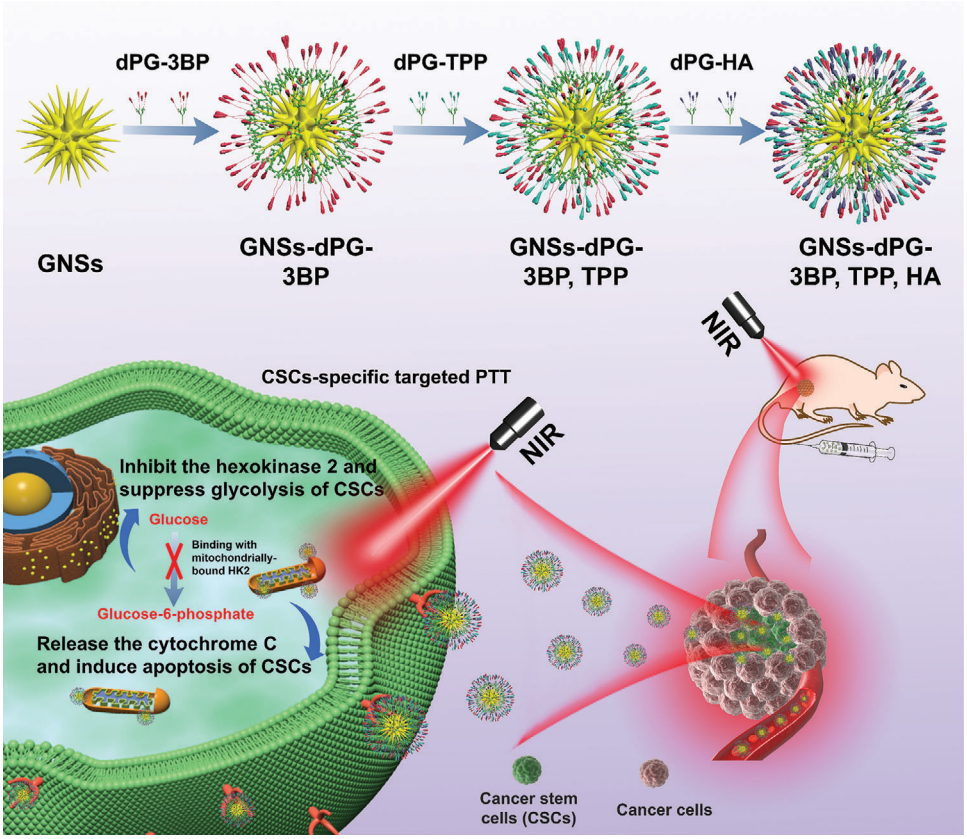


**Figure 1.** Synthetic scheme of GNSs-dPG-3BP, TPP, HA nanocomposite particles for metabolism inhibition and targeted PTT in breast CSCs.

74.5 °C and after a rapid 5 min rise, the temperature reached a plateau. Moreover, the different dPG conjugations did not affect the photothermal performance, the temperature variation of various GNSs nanocomposite particles was similar and exhibited negligible variations. The corresponding thermal imaging photographs were also illustrated in Figure 2e, which were consistent with the temperature curves. These results indicated that the as-prepared GNSs and various GNSs nanocomposite particles had excellent photothermal performance upon laser irradiation, which encouraged us to employ the GNSs nanocomposite particles for the further PTT therapeutic in CSCs.

### 2.2. In Vitro Cellular Uptake

The cellular uptake and intracellular distribution of the nanocomposite particles are key factors in determining the therapeutic efficacy of CSCs. In particular, the binding affinity to the HK2 and mitochondria are very important to the metabolism inhibition. The CSCs targeting capability plays a major role in PTT therapeutic efficacy against CSCs. Since the CSCs are located in the internal center of solid tumors, therefore the in vitro three-dimensional mammosphere cell culture is more suitable to mimic complex physiological conditions of CSCs in tumors than two-dimensional cell culture.[39,40] More importantly, the mammosphere cells, which had been enriched with breast CSCs and highly expressed the CD44 membrane protein, could specifically bind by HA.[32] The morphology of mammosphere cells was displayed as clustered round shape, which was different from 2D-cultured cells. The mammosphere cells were utilized to determine the cellular uptake and targeting penetration capacity of the designed nanocomposite particles to CSCs in this study.

We incubated GNSs-dPG, GNSs-dPG-3BP, GNSs-dPG-3BP, TPP and GNSs-dPG-3BP, TPP, HA with mammosphere cells for 4 h first, and then investigated by ICP, flow cytometry, and CLSM. First, the overall intracellular accumulation of gold was quantified using the ICP measurement, as shown in **Figure 3**a. The intracellular accumulation amount in the cells incubated with GNSs-dPG-3BP was slightly higher than the GNSs-dPG. Due to the mitochondria targeting by TPP, the GNSs-dPG-3BP, TPP showed significant enhancement in the intracellular accumulation amount. Especially with the help of HA, which targeted to CSCs, the cellular uptake of GNSs-dPG-3BP, TPP, and HA was significantly boosted, and has shown four times higher accumulation compared to GNSs-dPG, which was favorable for their therapeutic applications in CSCs.

Moreover, to evaluate the cellular uptake and targeting capability by flow cytometry and CLSM, the various GNSs nanocomposite particles were labeled with the fluorescent probe IDCC first. The cellular uptake of the nanocomposite particles, which was characterized by flow cytometry, was realized by measuring the fluorescence intensity of IDCC. The flow cytometry curves were shown in Figure 3b, in which the fluorescence intensity of GNSs-

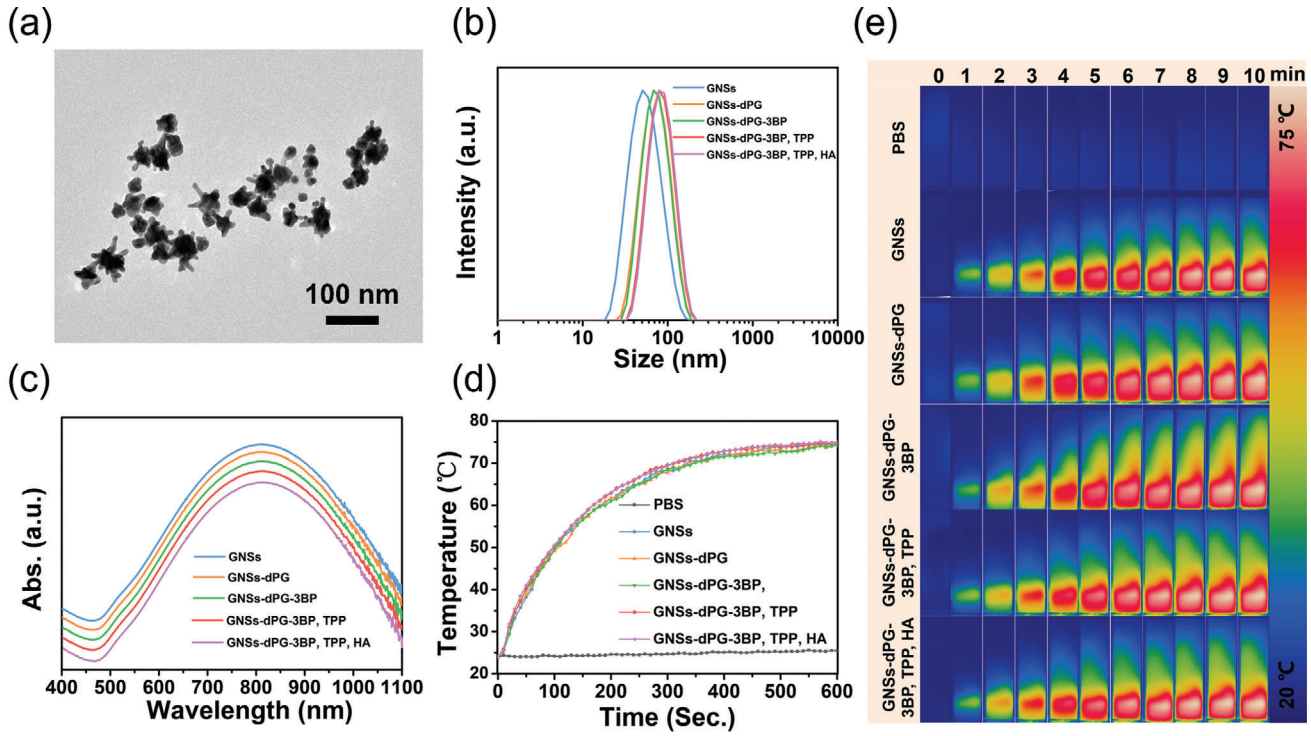


**Figure 2.** a) TEM images of the GNSs. b,c) DLS curves and UV-vis absorption spectra of GNSs, GNSs-dPG, GNSs-dPG-3BP, GNSs-dPG-3BP, TPP and GNSs-dPG-3BP, TPP, HA nanocomposite particles. d,e) Temperature variation and the corresponding IR thermal imaging of PBS, GNSs, GNSs-dPG, GNSs-dPG-3BP, GNSs-dPG-3BP, TPP, and GNSs-dPG-3BP, TPP, HA nanocomposite particles upon laser irradiation.

dPG-3BP was slightly stronger than that of GNSs-dPG. Moreover, a significantly stronger fluorescence intensity was observed in GNSs-dPG-3BP, TPP, which indicated mitochondria targeting by TPP increased the accumulation of nanocomposite particles in the mammosphere cells. Notably, the fluorescence intensity in cells incubated with GNSs-dPG-3BP, TPP, and HA was stronger than that of GNSs-dPG-3BP, TPP, which suggested the HA modification could improve the accumulation. These results were also consistent with the ICP results.

Furthermore, the CLSM was used to observe the cellular uptake and internalization of various nanocomposite particles. As depicted in Figure 3c, the red fluorescence represented the intracellular nanocomposite particles labeled by IDCC, the blue fluorescence represented the nuclei, and the green fluorescence of FITC represented the cytoskeleton. The internalization of the GNSs-dPG could easily be observed, which was mainly located in the cytoplasm. Importantly, it was found that GNSs-dPG-3BP, and GNSs-dPG-3BP, TPP nanocomposite particles could accumulate in mammosphere cells much more than GNSs-dPG, which attributed to the binding of HK2 with 3BP and the mitochondria targeting by TPP. Stronger fluorescence of the GNSs-dPG-3BP, TPP, and HA nanocomposite particles was observed in the mammosphere cells, which indicated that the internalization of GNSs-dPG-3BP, TPP, HA was obviously enhanced. With the HA modification, the GNSs-dPG-3BP, TPP, HA could penetrate into the center of the mammosphere cells more easily, suggesting that the binding and targeting between the HA and the CD44 overexpressed CSCs were stronger. The superior targeting and penetration capacity of GNSs-dPG-3BP, TPP, HA may provide a greater opportunity to approach the CSCs and promote the therapeutic efficacy of CSCs.

It has been reported that the HK2 was upregulated in cancer cells and highly bind with mitochondria to obtain the ATP for accelerating the glycolytic rate.[11,12] The 3BP could selectively suppress the glycolytic capacity of cancer cells by inhibiting mitochondrial-bound HK2. Therefore, the association between HK2 and mitochondria was investigated in the mammosphere cells using CLSM, which is illustrated in **Figure 4**b, the HK2 and mitochondria were stained as red and green fluorescence, respectively. It could be clearly observed that the majority of HK2 was bound to mitochondria, which meant that mitochondria targeting would improve the HK2 inhibition by 3BP.

The intracellular distribution of the nanocomposite particles is very important for the therapeutic efficacy of CSCs, especially the binding affinity of our nanocomposite particles to HK2 and mitochondria is the key factor for metabolism inhibition. Therefore, to verify the intracellular binding affinity of the nanocomposite particles to HK2 and mitochondria in mammosphere cells, the HK2 and mitochondria were stained with green fluorescence first, and the different layers of the mammosphere cells were observed using CLSM by varying the z-axis (Figure 4a, S2, and S3, Supporting Information). As shown in Figure 4c–g, there were negligible GNSs-dPG nanocomposite particles binding with HK2. However, GNSs-dPG-3BP could bind with HK2 more easily than GNSs-dPG, suggesting that the 3BP modification has improved the binding affinity to HK2. Furthermore, due to active mitochondria targeting and the mitochondrial-bound HK2, the GNSs-dPG-3BP, TPP nanocomposite particles were up-

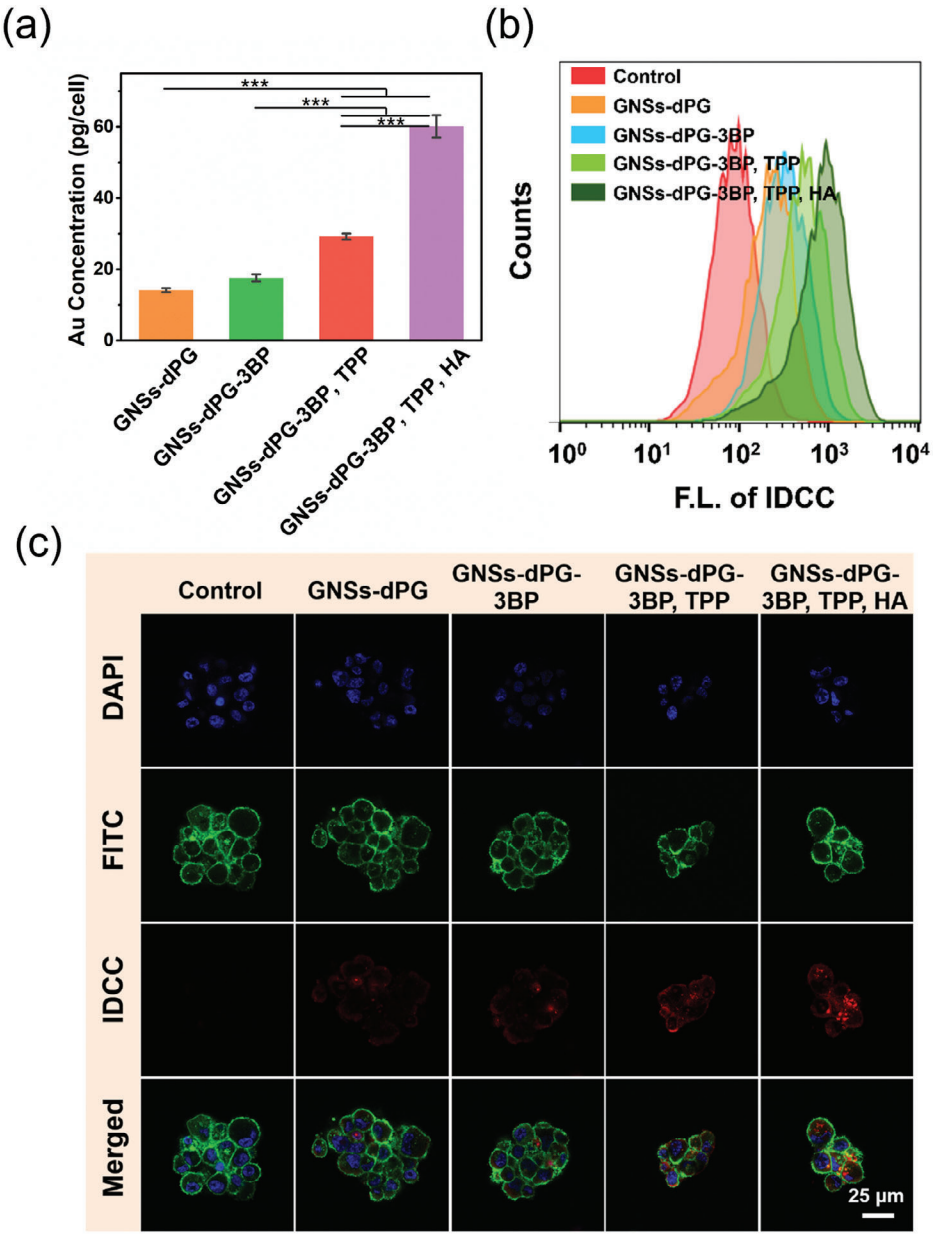


**Figure 3.** a) The degree of cellular uptake quantified by ICP. Results are represented as mean ± SD ($n = 3$). b) Flow cytometry curves and c) CLSM images of mammosphere cells incubated with various nanocomposite particles (PBS, GNSs-dPG, GNSs-dPG-3BP, GNSs-dPG-3BP, TPP and GNSs-dPG-3BP, TPP, HA) by measuring IDCC fluorescence.

taken by mammosphere cells significantly higher than GNSs-dPG-3BP. Notably, more GNSs-dPG-3BP, TPP, and HA could bind with HK2, which suggests that the HA modification could greatly improve the attachment and internalization of GNSs-dPG-3BP, TPP, HA. The same situation could be observed in the mitochondria staining results (Figure 4h–l). Where the few GNSs-dPG and GNSs-dPG-3BP nanocomposite particles were bound with mitochondria, while with the mitochondria targeting by TPP, abound GNSs-dPG-3BP, TPP nanocomposite particles were found in the mammosphere cells. With the HA targeting, more GNSs-dPG-3BP, TPP, and HA were uptaken by the cells. In addition, the nanocomposite particles were observed at different layers of the mammosphere from top to bottom, owing to the fact that CSCs were located in the inner region of solid tumors. This indicated that our prepared nanocomposite particles could penetrate into the center of the tumor and reach the CSCs.

### 2.3. In Vitro Photothermal Therapy of CSCs

The designed nanocomposite particles mediated in vitro PTT therapeutic performance on CSCs was evaluated via the CCK8 assay. In brief, the mammosphere cells were irradiated with 808 nm laser for 5 min after incubating with GNSs-dPG, GNSs-dPG-3BP,

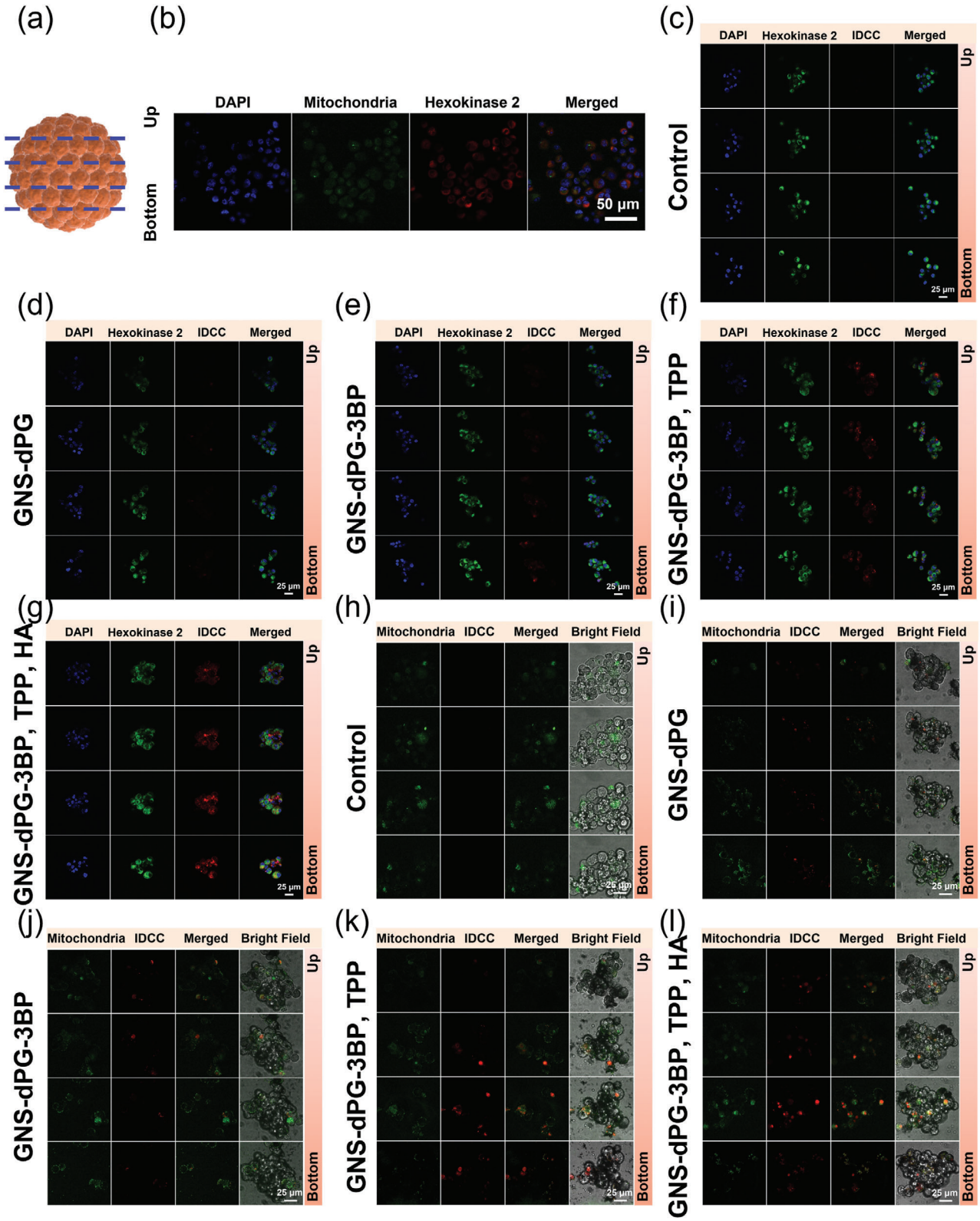


**Figure 4.** a) Cartoon reflects the images change of the depth along the z-axis in mammosphere cells from up to bottom. b) Mitochondrial and HK2 localization in mammosphere cells as demonstrated by confocal immunofluorescence microscopy. (c-l) The HK2 and mitochondria-targeted cellular uptake of various nanocomposite particles, confocal immunofluorescence microscopy images of the mammosphere cells incubated with c, h) PBS, d, i) GNSs-dPG, e, j) GNSs-dPG-3BP, f, k) GNSs-dPG-3BP, TPP and g, l) GNSs-dPG-3BP, TPP, HA, by measuring HK2 (green), mitochondria (green) and IDCC fluorescence (red) at different layers.

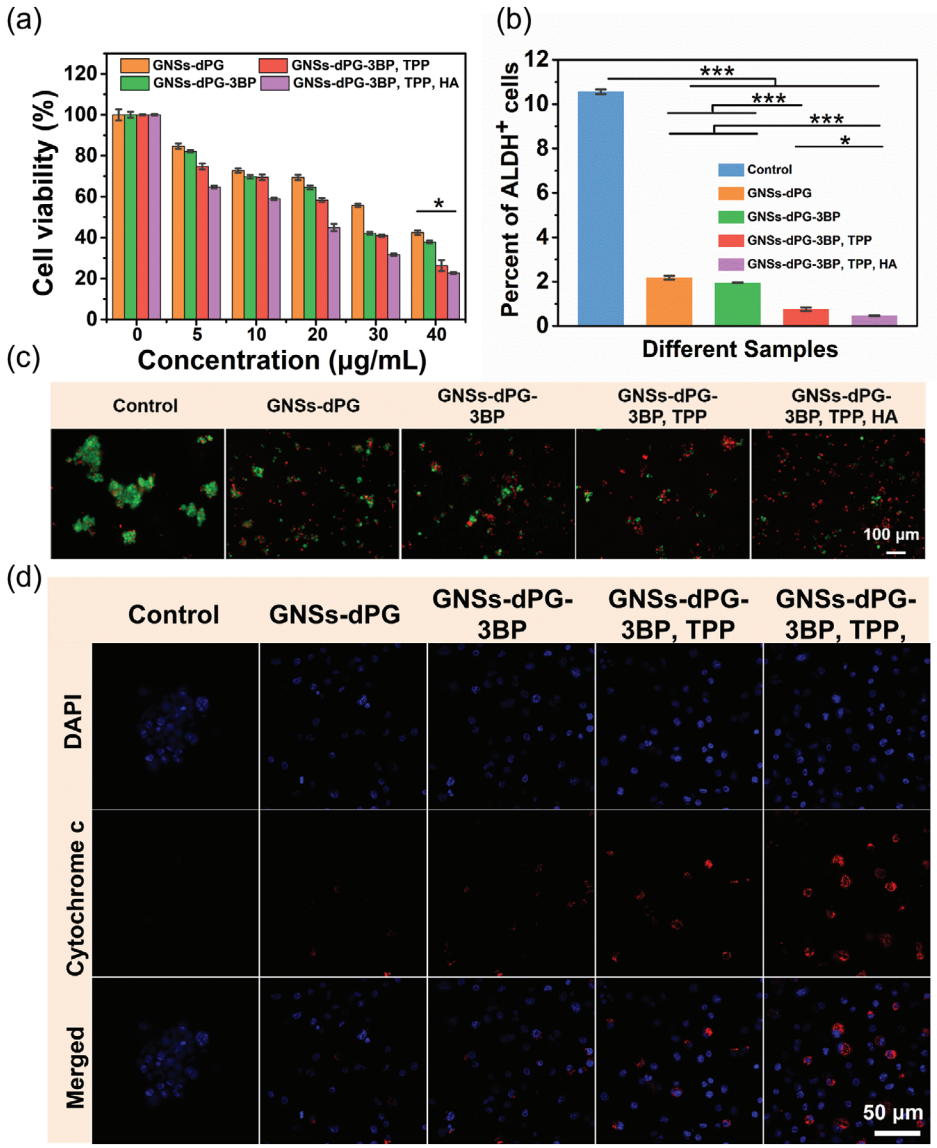


**Figure 5.** In vitro viabilities of mammosphere cells treated with various nanocomposite particles (PBS, GNSs-dPG, GNSs-dPG-3BP, GNSs-dPG-3BP, TPP and GNSs-dPG-3BP, TPP, HA) under 808 nm laser irradiation characterized by a) the CCK8 assay and c) live/dead cell staining (as green/red color). b) Statistic results of flow cytometry analysis of $ALDH^+$ in mammosphere cells treated with various nanocomposite particles under 808 nm laser irradiation. Results are represented as mean ± SD ($n = 3$). d) Cytochrome c immunofluorescence of mammosphere cells treated with various nanocomposite particles under 808 nm laser irradiation.

GNSs-dPG-3BP, TPP and GNSs-dPG-3BP, TPP, HA nanocomposite particles with 0. 5, 10, 20, 30, 40 μg $ml^{-1}$ of gold, then the cell viability was characterized. As shown in **Figure 5**a, the viability of mammosphere cells incubated with GNSs-dPG was decreased gradually with an increase in concentration, and the viability was measured to be 42.5% at a gold concentration of 40 μg $ml^{-1}$. Furthermore, more mammosphere cells were killed corresponding to the GNSs-dPG-3BP and GNSs-dPG-3BP, TPP under the same condition, in which the viability was 37.9% and 26.3%, respectively, indicating that 3BP modification and the TPP targeting would promote the PTT efficacy. It is noteworthy that the GNSs-dPG-3BP, TPP, and HA exhibited the highest toxicity, the cell viability was the worst and decreased to 22.7%, which could be attributed to enhanced uptake of nanocomposite particles owing to the HA targeting and further improve the PTT efficacy. The results illustrated that GNSs-dPG-3BP, TPP, and HA have excellent in vitro PTT therapeutic performance.

The number of CSCs is related to the malignancy and invasiveness of the tumor.[2] Therefore, it is very important to investigate the amount of CSCs subpopulation after the treatment. ALDH has been proven as a specific intracellular marker of CSCs, in which the $ALDH^+$ phenotypes have the CSCs cancer-initiating characteristics.[20] The $ALDH^+$ proportion of mammosphere cells was investigated via flow cytometry after treatment with the designed nanocomposite particles mediated PTT. As shown in Figure 5b, the untreated mammosphere cells showed the $ALDH^+$

proportion of about 10.5%. After treatment with GNSs-dPG and GNSs-dPG-3BP mediated PTT, the percentage of $ALDH^+$ cells were significantly decreased to 2.2% and 1.9%. However, when the GNSs-dPG-3BP, TPP exposed mammosphere cells were under the laser irradiation, the $ALDH^+$ proportion decreased to 0.8%, which indicates the enhancement in therapeutic efficacy in the presence of TPP. The GNSs-dPG-3BP, TPP, and HA mediated PTT showed the lowest $ALDH^+$ proportion (0.5%), which is attributed to increased targeting uptake by CSCs, therefore it eliminates the CSCs more efficiently. The decrease of the $ALDH^+$ proportion demonstrated that GNSs-dPG-3BP, TPP, and HA mediated PTT have great potential for CSCs elimination and cancer-initiating inhibition.

In order to confirm the effect of the designed nanocomposite particles mediated in vitro PTT therapeutic performance, the in vitro IR thermal imaging was characterized. As shown in Figures S4 and S5, Supporting Information, the mammosphere cells were incubated with the designed nanocomposite particles first, then irradiated with 808 nm laser, the heating curves and corresponding thermal imaging photographs were recorded. Under 808 nm laser irradiation, the temperature of mammosphere cells incubated with GNSs-dPG could increase to about 60.2 °C, which is sufficient to destroy the mammosphere cells. Furthermore, the increased temperature of GNSs-dPG-3BP and GNSs-dPG-3BP, TPP was significantly higher than GNSs-dPG, which would kill the mammosphere cells more efficiently. In the case of the mammosphere cells incubated with GNSs-dPG-3BP, TPP, and HA, the temperature variation shows the highest increase, suggesting the combined targeting effects of 3BP, TPP and HA, that could enhance the PTT therapeutic efficiency on CSCs. Considering the negligible difference in photothermal performance of the various GNSs nanocomposite particles, the PTT therapeutic effect is related to the cellular uptake dose, suggesting specific CSCs targeting could greatly improve the PTT therapeutic efficiency.

Furthermore, to intuitively characterize the designed nanocomposite particles mediated in vitro PTT therapeutic performance on CSCs, the live and dead cells were stained by CAM/EthD-1 agents. As shown in Figure 5c, the control mammosphere cells were alive, and cell death was observed when treated with GNSs-dPG. However, more dead cells could be observed for GNSs-dPG-3BP, significant cell death and destroyed mammosphere were observed for GNSs-dPG-3BP, TPP. Moreover, the cells treated with GNSs-dPG-3BP, TPP, and HA resulted in a significant scattered and decreased mammosphere, which have the best PTT performance.

The interactions between HK2 and mitochondria not only affect the metabolism, but also suppress the release of cytochrome c, which is a critical step in the apoptotic pathway, therefore resulting in CSCs resistance to apoptosis. As a result, with the help of HK2 inhibition ability by 3BP and the PTT treatment, the release of cytochrome c will increase and subsequently induce cell apoptosis. To determine the effect of designed nanocomposite particles mediated treatment on the cytochrome c release, we performed the immunocytochemical staining of cytochrome c. As shown in Figure 5d, the expression of cytochrome c was observed in cells incubated with GNSs-dPG. Furthermore, increased expression levels were observed in GNSs-dPG-3BP treated cells, and GNSs-dPG-3BP, TPP treated cells showed a more significant increased expression that demonstrated the mitochondria targeting by TPP could enhance the inhibition of HK2 and result in an increase of cytochrome c release. Consistent with the above findings, owing to CSCs active-targeting HA, the GNSs-dPG-3BP, TPP, and HA treated cells had the best therapeutic efficiency, and even more significant cytochrome c could be observed. These results suggest that with the inhibition of HK2, the interaction between HK2 and mitochondria could be disrupted after the CSCs were treated by GNSs mediated PTT. It results in a dramatic increase of the cytochrome c release and subsequently induces cell apoptosis.

### 2.4. Inhibiting the Expression of Stemness-Associated Gene of CSCs and In Vitro Mammospheres Formation Assay

After the treatment as described above, the stemness-related genes expression of the manmosphere cells was determined by measuring the CSCs-associated genes (SOX2, NANOG, and OCT4) using qRT-PCR. As shown in **Figure 6**a–c, the expressions of SOX2, NANOG, and OCT4 were decreased in cells treated with GNSs-dPG. Moreover, with the HK2 binding and mitochondria targeting ability, the stemness genes expressions of GNSs-dPG-3BP and GNSs-dPG-3BP, TPP treated cells were markedly suppressed. Importantly, GNSs-dPG-3BP, TPP, and HA treated cells demonstrate more significant suppression of the expression of stemness associated genes, indicating that the CSCs targeting molecule HA conjugation would evidently improve the suppression effect. This result suggests that PTT treatment based on GNSs-dPG-3BP, TPP, and HA nanocomposite particles are very effective in suppressing expression of CSCs-associated genes, which is very important for eliminating CSCs.

To investigate the effect of the designed nanocomposite particles mediated PTT on CSCs elimination, the mammospheres formation assay was employed. The decreased CSCs proportion would prohibit mammosphere formation ability from CSCs, which is regarded as a characteristic of CSCs.[32] After incubation with various nanocomposite particles, the primary mammospheres cells were treated with laser irradiation, then the cells were collected and re-plated in suspension culture for 10 days to form mammospheres. The formed secondary mammospheres were counted and imaged. As shown in Figure 6d,e, abundant mammospheres could be observed in the control, while cells treated with GNSs-dPG mediated PTT decreased the amount of secondary mammospheres, generating small and fragmentary mammosphere. Moreover, a significant reduction in secondary mammosphere formation could be observed in cells treated with GNSs-dPG-3BP and GNSs-dPG-3BP, TPP. Furthermore, few secondary mammospheres were formed after the treatment of GNSs-dPG-3BP, TPP, and HA mediated PTT, and the number of the formed mammospheres also decreased, which suggested HA targeting significantly diminished the mammosphere formation ability and eliminated more CSCs efficiently.

### 2.5. In Vivo Bio-Distribution, In Vivo Photothermal Effect and PTT Therapeutic Effect Evaluation

High biocompatibility is vital factor for in vivo biomedical applications of the nanocomposite particles. The biocompatibility of

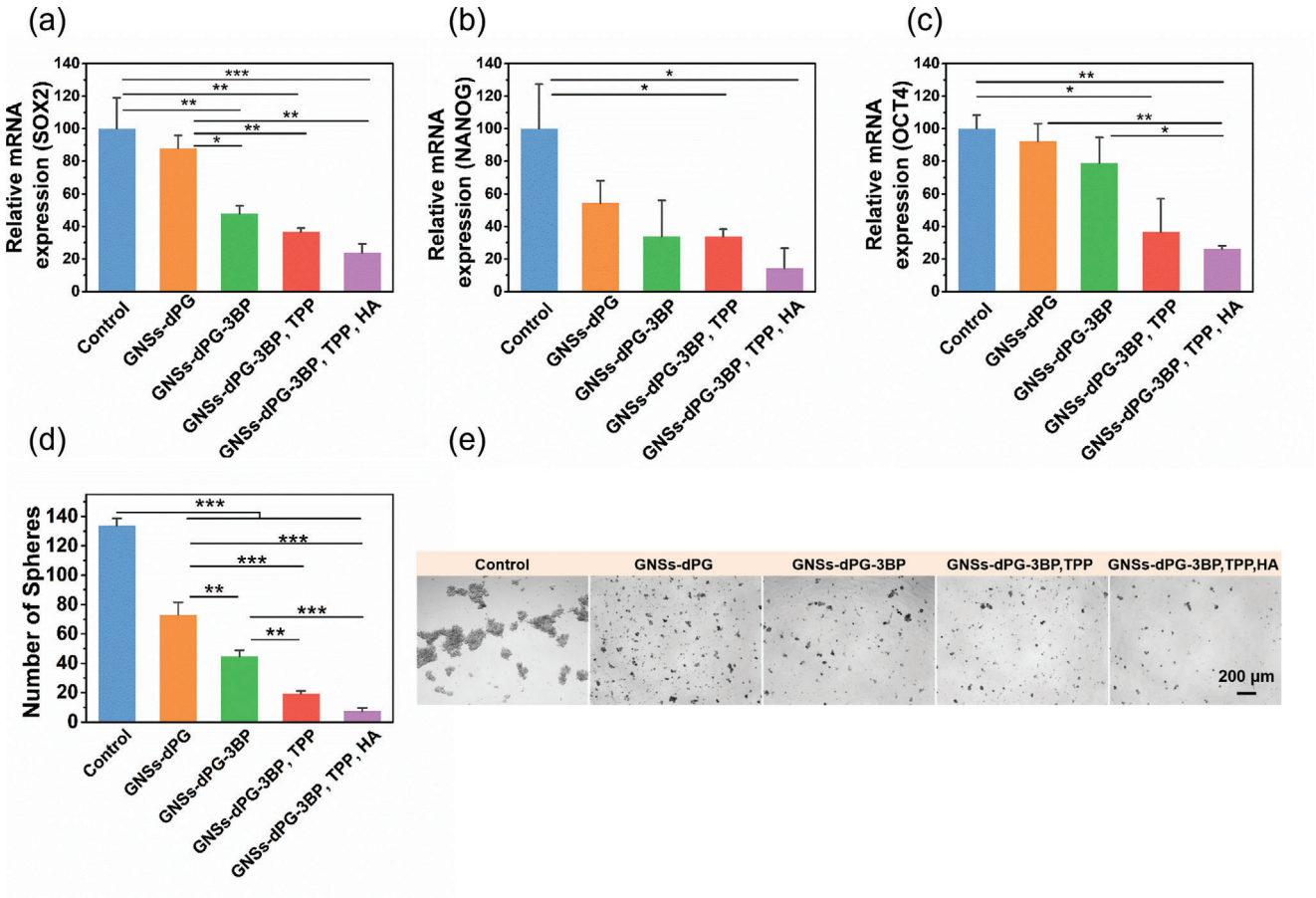


**Figure 6.** a–c) The expression of stemness-associated genes (SOX2, NANOG, and OCT4) in mammosphere cells after the treatment with various nanocomposite particles. d,e) After the treatment, the cells were seeded and maintained for 10 days for secondary mammospheres formation assay, then counted the number of mammospheres (>50 μm) and taken the optical micrographs. Results are represented as mean ± SD ($n = 3$).

the nanocomposite particles was evaluated by H&E staining analysis of major organs in healthy nude mice. Briefly, the healthy nude mice were injected with PBS, GNSs-dPG-3BP, GNSs-dPG-3BP, TPP and GNSs-dPG-3BP, TPP, HA via the tail vein, after four weeks, the major organs (heart, liver, spleen, lung, and kidney) were analyzed by H&E staining. As depicted in Figure S6, Supporting Information, no evident tissue damage in histological specimens were observed at this injection dose, and obvious morphology change in the major organs was not found. The results indicated that the nanocomposite particles had good biocompatibility and could be safe for biomedical applications.

To explore the potential applications in vivo and verify whether the designed nanocomposite particles could accumulate in tumors, the in vivo bio-distribution of two nanocomposite particles was investigated. The tumor-bearing mice were intravenously injected with GNSs-dPG-3BP and GNSs-dPG-3BP, TPP, HA. The gold concentration in tumor and the main organs (including heart, liver, spleen, lung, and kidney) were analyzed by using ICP-MS at 24 h post injection. As illustrated in **Figure 7**a, the designed nanocomposite particles could accumulate in the tumor tissue due to the enhanced permeability and retention (EPR) effect. Encouragingly, the accumulation amount of GNSs-dPG-3BP, TPP, HA in tumors was found to be obviously higher than GNSs-dPG-3BP, confirming the significant CSCs targeting ability of GNSs-dPG-3BP, TPP, HA in vivo. And considerable nanocomposite particles were accumulated in liver and spleen owing to the macrophage phagocytosis. In contrast, only few nanocomposite particles were detected in the heart, lung, and kidney. This result demonstrated that the designed nanocomposite particles could efficiently target the tumor site due to the appropriate particle size and surface targeting ligand modification, by passive and active targeting.

Given the above tumor accumulation results, the GNSs-dPG-3BP, TPP, and HA can be used as an ideal CSCs targeted PTT therapeutic probe. To evaluate the in vivo photothermal effect of the designed nanocomposite particles, the tumor-bearing mice were intravenous injected with PBS, GNSs-dPG-3BP, GNSs-dPG-3BP, TPP and GNSs-dPG-3BP, TPP, HA, and then exposed to 808 nm laser irradiation at 24 h post injection. The thermal images were taken by an infrared thermal camera during the irradiation to detect the tumor temperature at different time points. As shown in Figure 7b,c, the PBS injected tumors exhibited a slight temperature change, which suggested a negligible heating effect of the laser on mice. In contrast, the GNSs-dPG-3BP-treated tumors experienced a temperature rise to 48.9 °C over the course of 5 min irradiation. It is noted that the GNSs-dPG-

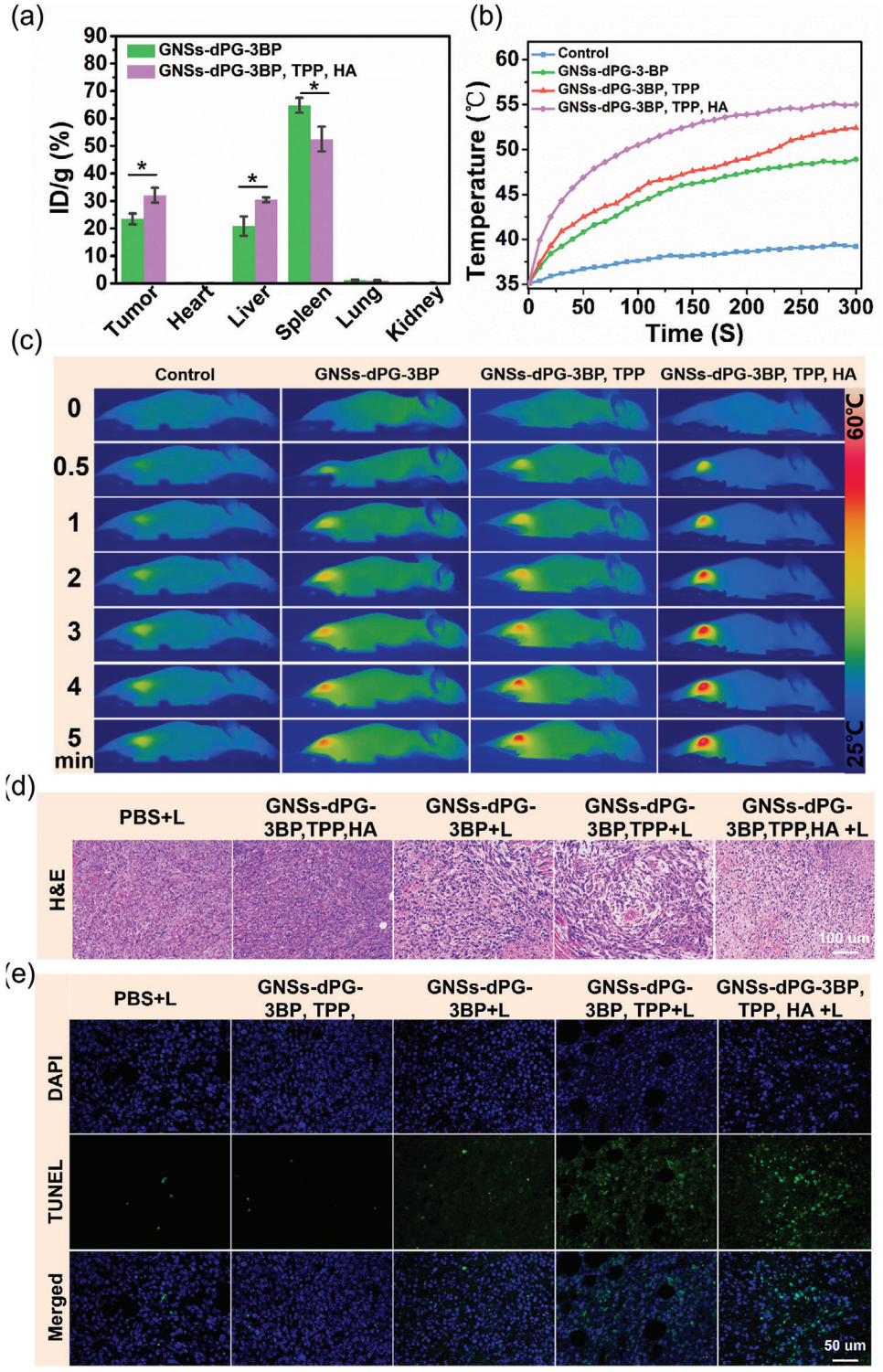


**Figure 7.** a) Bio-distribution of nanocomposite particles in different organs of 4T1 tumor-bearing nude mice at 24 h post i.v. injection with GNSs-dPG-3BP, TPP and GNSs-dPG-3BP, TPP, HA quantified by ICP-OES measurement. Results are represented as mean ± SD ($n = 3$). b,c) The temperature variation and the corresponding IR thermal imaging of 4T1 tumor-bearing mice at 24 h post i.v. injection of PBS, GNSs-dPG-3BP, GNSs-dPG-3BP, TPP and GNSs-dPG-3BP, TPP, HA upon 808 nm laser irradiation (1.5 W $cm^{-2}$). d,e) H&E and TUNEL staining of the sliced tumors from 4T1 tumor-bearing mice, which underwent 808 nm laser exposure (1.5 W $cm^{-2}$, 5 min) at 24 h post i.v. injection of PBS or various nanocomposite particles, the tumors were dissected for staining 24 h after the treatment.

3BP, TPP and GNSs-dPG-3BP, TPP, HA-injected tumors exhibited a higher temperature increase, reaching 52.5 and 55.0 °C after 5 min laser irradiation, which is high enough to ablate and destroy the CSCs. This observation demonstrated that the enhanced accumulation by active targeting would improve the PTT therapeutic efficiency. The thermal images of the tumor changed from blue to red during the increasing tendency of temperature. Therefore, the results revealed GNSs-dPG-3BP, TPP, and HA may serve as an efficient CSCs-targeted PTT therapeutic probe in vivo.

Afterward, to further evaluate the therapeutic effect of the designed nanocomposite-mediated treatment in vivo, the 4T1 and MDA-MB-231 tumor-bearing model of nude mice were established. The 4T1 and MDA-MB-231 cell lines have been proven that they possess an increased CSCs subpopulation, which is a good candidate for in vivo CSCs xenograft tumor model research.[41] The tumor-bearing nude mice were divided into five groups and intravenously injected: PBS with laser irradiation (PBS + L), GNSs-dPG-3BP, TPP, and HA without laser irradiation (GNSs-dPG-3BP, TPP, and HA), GNSs-dPG-3BP with laser irradiation (GNSs-dPG-3BP + L), GNSs-dPG-3BP, TPP with laser irradiation (GNSs-dPG-3BP, TPP + L) or GNSs-dPG-3BP, TPP, HA with laser irradiation (GNSs-dPG-3BP, TPP, HA + L). The tumors were exposed to 808 nm laser irradiation for 5 min at 24 h post-injection. Subsequently, 24 h after the treatments, the tumors were harvested and recorded by real photographs, then sliced for hematoxylin and eosin (H&E) staining and terminal deoxynucleotidyl transferase dutp nick end labeling (TUNEL) staining.

As shown in Figures S7 and S8, Supporting Information, no palpable change or damage was observed in mice injected with PBS under the laser irradiation or only injected with GNSs-dPG-3BP, TPP, and HA. However, the tumor sites of the other three groups showed prominently necrosis and damaged areas. The tumor shrinkage and dark colors could be observed clearly in treatment center. These results demonstrated that the elevated temperature induced by the PTT therapeutic effect was high enough to destroy the tumor tissue.

Moreover, the H&E and TUNEL staining of the tumors were carried out to evaluate the necrotic and apoptotic cells after the nanocomposite-mediated treatment in vivo. As shown in Figure 7d,e, 4T1 tumor-bearing nude mice treated with PBS + L and GNSs-dPG-3BP, TPP, HA were not showing obvious tumor necrosis and pathological damage in H&E staining images, and the TUNEL staining was negative. However, in GNSs-dPG-3BP + L treated tumor, the sporadic necrotic and apoptotic areas were revealed in H&E and TUNEL staining results. Furthermore, large areas of tumor necrosis and apoptosis could be observed in GNSs-dPG-3BP, TPP + L treated tumor, which indicated the advantage of mitochondria targeting. Notably, the extensive necrosis, the majority of damaged cancer cells, and significant apoptosis appeared in tumors treated with GNSs-dPG-3BP, TPP, HA + L, which suggested that the mitochondrial-bound HK2 targeting induced metabolism inhibition and targeted ablation of CSCs would enhance the therapeutic efficacy. As shown in Figure S9 and S10, Supporting Information, similar to the results of 4T1 tumor-bearing nude mice, apparent extensive necrosis and apoptosis also existed in MDA-MB-231 tumor-bearing nude mice after the treatment. These results suggested that the designed nanocomposite-mediated treatment could effectively destruct the tumor in both 4T1 and MDA-MB-231 tumor-bearing CSCs xenograft tumor model. Based on these results, the remarkable necrosis and apoptosis induced by treatment would enhance the CSCs therapeutic efficacy and further suppress the tumor growth.

The existence of CSCs would initiate metastatic tumor formation, thereby reducing the therapeutic efficacy of the ongoing treatment and making the treatment unsuccessful.[3] To investigate the in vivo anti-CSCs capacity of the designed nanocomposite particles, we analyzed the CSCs expression in the tumors with immunohistochemical (IHC) staining of CSCs marker CD44, NANOG, and SOX2 after the in vivo treatments. As shown in **Figure 8**a–c and Figure S11–S13, Supporting Information (4T1 and MDA-MB-231 tumor-bearing nude mice, respectively), the expression of the three CSCs marker in tumors treated with the PBS + L and GNSs-dPG-3BP, TPP, and HA were high and comparable. Moreover, both the GNSs-dPG-3BP + L and GNSs-dPG-3BP, TPP + L treatments evidently reduced the ratio of CSCs. More importantly the tumor treated with GNSs-dPG-3BP, TPP, HA + L showed the best depletion of CSCs, which exhibited a dramatic decrease on the expression of the CSCs marker. These results demonstrate that GNSs-dPG-3BP, TPP, HA nanocomposite particles can be used as in effectively targeting and eliminating the breast CSCs in vivo, which was attributed to its excellent mitochondrial-bound HK2 targeting induced metabolism inhibition and CSCs targeted-photothermal ablation effect.

### 2.6. In Vivo PTT

The CSCs could initiate tumor formation and have an influence on tumor growth. The in vivo therapeutic efficacy of CSCs was further explored by assessing tumor growth curves for 14 days. The tumor-bearing nude mice were randomly divided into five groups, then intravenously injected, and treated with PBS + L, GNSs-dPG-3BP, TPP, GNSs-dPG-3BP + L, GNSs-dPG-3BP, TPP + L and GNSs-dPG-3BP, TPP, HA + L, respectively. The tumor volumes of mice were measured every other day after treatment. As depicted in **Figure 9**a, tumor growth for treatments with GNSs-dPG-3BP, TPP, and HA was slightly inhibited compared to the PBS + L treated control, which would be attributed to the inhibition of metabolism. While without laser irradiation, the slight tumor suppression could not affect the tumor growth rate. The group treated with GNSs-dPG-3BP + L shown inhibition of tumor growth, and the tumor growth in the GNSs-dPG-3BP, TPP + L treated group was further slowed down, thereby demonstrating a more effective tumor inhibition. These results indicated that the mitochondrial-bound HK2 targeting induced metabolism inhibition together with the PTT could effectively inhibit tumor growth. Although the tumor suppression was realized by GNSs-dPG-3BP + L and GNSs-dPG-3BP, TPP + L treatment, while the tumor showed continued regrowth from day 6 owing to the incomplete apoptosis and the survival of CSCs. In sharp contrast, with the CSC-targeting advantage, GNSs-dPG-3BP, TPP, and HA + L exhibited the best anti-tumor capacity, the tumor growth was remarkably suppressed. The results demonstrated that GNSs-dPG-3BP, TPP, HA nanocomposite particles have an extraordinary capability for effectively eliminating the CSCs and

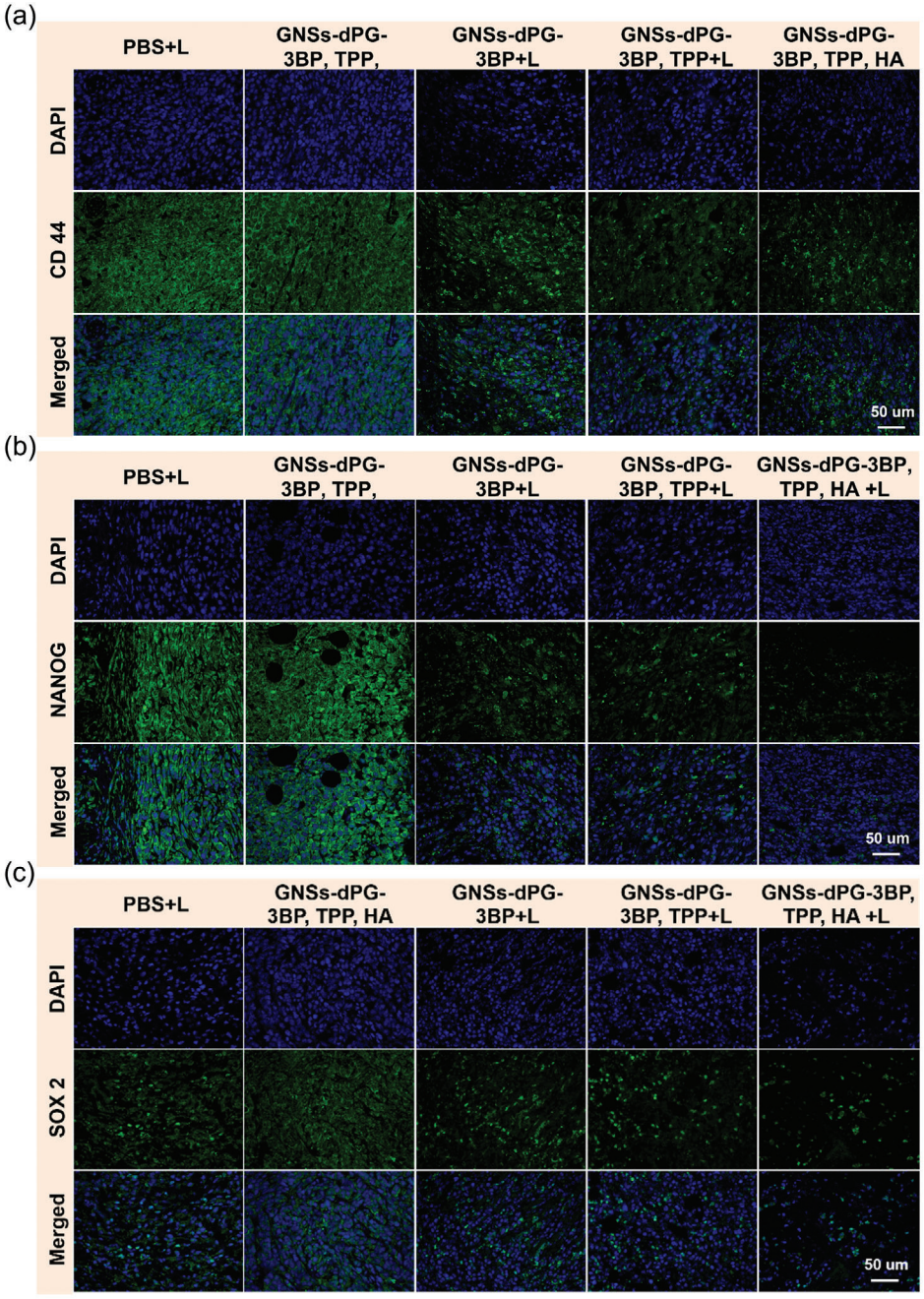


**Figure 8.** (a) CD44, (b) NANOG, and (c) SOX2 immunohistochemical staining of the sliced tumors from 4T1 tumor-bearing mice, which underwent 808 nm laser exposure (1.5 W $cm^{-2}$, 5 min) at 24 h post i.v. injection of PBS or various nanocomposite particles, the tumors were dissected for staining 24 h after the treatment.

excellent in vivo therapeutic efficiency. The in vivo inhibition of tumor growth was attributed to mitochondrial-bound HK2 targeting induced metabolism inhibition and targeted ablation of CSCs by hyperthermia. These results were consistent with the results of in vitro viability assays. Moreover, the real photographs of tumor-bearing nude mice in different groups were taken, which clearly showed the variations of tumor volume at different days (Figure 9e). Subsequently, tumors were harvested and weighed on the final day (Figure 9c), which corresponded with the in vivo results of tumor suppression. The in vivo therapeutic results concluded that GNSs-dPG-3BP, TPP, and HA could coordinate PTT with metabolism inhibition, obtain excellent in vivo anti-cancer efficiency on CSCs and have potential for clinical applicability as CSCs-targeted therapeutic nanocomposite particles.

Moreover, to assess the risk and toxicity of the treatment, the body weight was recorded every two days. Subsequently, at the end of the treatment, the major organs in mice were collected for histological analysis. As shown in Figure 9b, the treatments did

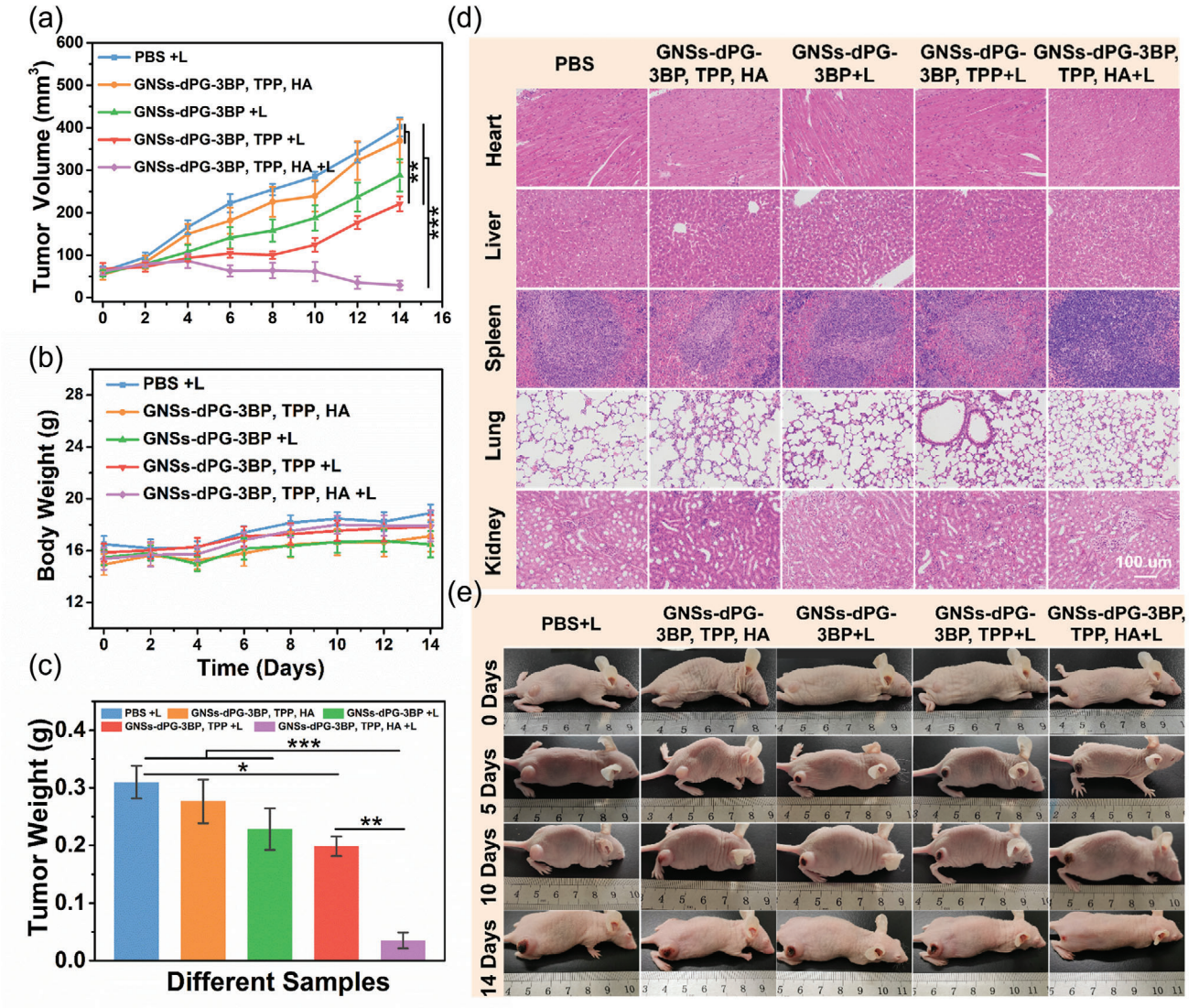


**Figure 9.** a) The change of relative tumor volume and b) body weight of the 4T1 tumor-bearing mice in each group ($n = 6$) after the treatment, recorded every 2 days. c) The tumors in each group were collected and weighed on day 14. d) H&E staining images of major organs (heart, liver, spleen, lung, and kidney) of tumor-bearing mice in each group on day 14. e) Representative digital images of the mice under different treatments on different days. Results are represented as mean ± SD ($n = 6$).

not lead to obvious side effects or significant body weight loss, implying the health condition of nude mice and excellent biocompatibility of the designed nanocomposite particles. In addition, as presented in Figure 9d, no evident tissue damage, and no obvious necrosis, fibrosis, or inflammatory were observed in the H&E stained tissue slices. This suggested that the major organs functioned properly and the minimal systemic toxicity in mice. These results preliminarily proved that the designed nanocomposite-mediated treatments were safe and had no acute toxicity to mice, which would have potential clinical application in CSCs therapy.

## 3. Conclusion

In summary, we have successfully developed GNSs-dPG-3BP, TPP, and HA nanocomposite particles, which exhibited metabolism inhibition and photothermal ablation ability. With the 3BP, TPP and HA decorated on the GNSs-dPG nanoplatforms, the nanocomposite particles exhibited superior binding ability with mitochondrial-bound HK2 and effective CSCs-specific targeted capability. Our results demonstrated that targeting the mitochondrial-bound HK2 via 3BP resulted in suppression of metabolism and further induced cellular apoptosis through the release of cytochrome c, which remarkably enhanced the therapeutic efficacy of PTT in breast CSCs and thus achieving a synergistic inhibitory effect. Moreover, the self-renewal of breast CSCs and the stemness gene expression were suppressed. The CSC-driven mammospheres formation was diminished after administrating the synergistic treatment. In addition, the in vivo tumor growth was effectively inhibited, and CSCs were eradicated, revealing effective tumor therapy of the nanocomposite

particles. Therefore, this work provided an attractive strategy and demonstrated a great potential for precise and highly efficient targeted eradication of CSCs.

## 4. Experimental Section

*Reagents*: Gold (III) chloride hydrate ($HAuCl_4 \cdot 4H_2O$), ascorbic acid, silver nitrate ($AgNO_3$), 1-ethyl-3-[3-dimethylaminopropyl] carbodiimide hydrochloride (EDC·HCl), N-hydroxysuccinimide (NHS), 3-bromopyruvic acid (3BP), 2-iminothiolane hydrochloride (Traut's reagent), and (4-Carboxybutyl) triphenylphosphonium bromide (TPP) were purchased from Merck. Sodium hyaluronate (HA, $M_w$ = 10 KDa) was purchased from Lifecore Biomedical (Chaska, MN, USA). dPG amino ($M_w$ = 5 kDa) was synthesized with 50% amination according to a previously published method by the group.[42] Dulbecco's modified Eagle's medium/Ham's nutrient mixture F12 (DMEM/F12), bovine serum albumin (BSA) and insulin were bought from Merck. Fetal bovine serum (FBS), Cell Light Mitochondria-GFP, BacMam 2.0, penicillin, and streptomycin were purchased from Invitrogen (USA). B-27 supplement, fibroblast growth factor-basic (FGF), and epidermal growth factor (EGF) were purchased from Thermo Fisher Scientific. The ALDEFLUOR kit was purchased from STEM CELL Technologies (Vancouver, Canada). All reagents were used as received. Milli-Q water (18.2 MΩ cm) was used in all experiments.

*Synthesis of GNSs-dPG-3BP, TPP, and HA Nanocomposite Particles*: The GNSs were prepared by a literature reported seed-mediated growth method.[43] The seed solution was synthesized by a citrate reduction method. Subsequently, 8 µl of the synthesized seed solution and 0.4 ml of 5 mM $HAuCl_4$ solution were mixed with 8 ml water under vigorous stirring (800 rpm), followed by the addition of 64 µl of $AgNO_3$ (10 mM) and 40 µl of freshly prepared ascorbic acid (100 mM) to the mixture simultaneously. After 30 s stirring, the solutions rapidly turned from light red to dark blue. To synthesize the GNSs-dPG-3BP, TPP, HA nanocomposite particles, the GNSs were modified with dPG-3BP, dPG-TPP, and dPG-HA, respectively. For dPG-3BP, dPG-TPP and dPG-HA preparation, the 3BP, TPP, and HA were conjugated with dPG amine ($M_w$ = 5 kDa, with 50% amino functionality) by EDC/NHS activation technique via acylation reaction between the terminal carboxyl of 3BP, TPP, HA, and the amino group of dPG. In brief, 3BP (2.5 mg, 15 µmol carboxyl groups), TPP (6.7 mg, 15 µmol carboxyl groups), and HA (3 mg, 7.5 µmol carboxyl groups) were respectively mixed with 2.4 times theoretical amount of EDC·HCl and NHS, and then kept on stirring for 8 h to activate the carboxyl groups. After that, the activated 3BP, TPP, and HA were added into dPG amine solution (11 mg), respectively, and stirred for 24 h. The product of dPG-3BP, dPG-TPP, and dPG-HA was dispersed in 11 ml water and used for further modification of GNSs. The dPG-3BP, dPG-TPP, and dPG-HA containing extra amino functionalities available for conversion to thiols by Traut's reagent.[44] Briefly, dPG-3BP, dPG-TPP, and dPG-HA solution (0.25 ml) was mixed with Traut's reagent (0.07 mg) for 20 min and then added into the prepared GNSs solution under stirring. After stirring for 30 min, the prepared dPG-3BP, dPG-TPP, and dPG-HA containing thiols group were modified onto the surface of GNSs through Au-S bonds to obtain GNSs-dPG-3BP, TPP, and HA. Finally, the resultant GNSs-dPG-3BP, TPP, and HA were collected by centrifugation and redispersed in water.

*Photothermal Performance*: The photothermal performance of various GNSs nanocomposite particles was investigated by 808 nm laser and an infrared thermal imaging system (PI400, Optris, Germany). 1 ml of various GNSs nanocomposite particles (40 µg $ml^{-1}$) was transferred to cuvettes and irradiated under 808 nm laser (1.5 W $cm^{-2}$) for 10 min, the temperature value was recorded every 10 s, and the thermal imaging was mapped every minute.

*Characterization*: Transmission electron microscopy (TEM) images were obtained on a FEI Talos L120C electron microscope. The dynamic light scattering (DLS) and zeta potential experiments were characterized by Zetasizer Nano-ZS (Malvern Instruments). The UV–vis absorption spectra were conducted using a UV-vis spectrophotometer (Lambda 950, Perkin Elmer). Inductively coupled plasma optical emission spectrometry (ICP-OES) was performed with an Optima 2100 instrument from Perkin Elmer.

*Cell Culture*: The MDA-MB-231 cell line of human breast cancer was obtained from Sigma. The MDA-MB-231 human breast cancer cell line was cultured in DMEM/F12 supplemented with 10% FBS, 100 units $ml^{-1}$ of penicillin, and 100 µg $ml^{-1}$ of streptomycin at 37 °C with 5% $CO_2$. The mammosphere cells were obtained by three-dimensional suspension culture, MDA-MB-231 cells (20000 cells $ml^{-1}$) were cultured in ultralow attachment plates with serum-free DMEM/F12 supplemented with 0.4% BSA, 20 ng $ml^{-1}$ FGF, 20 ng $ml^{-1}$ EGF, 5 µg $ml^{-1}$ insulin, and B27. After 10 days of culture, the mammospheres were collected and then cultured for further experimental use.

*Cellular Uptake Assay*: To evaluate targeted cellular uptake by ICP, the mammosphere cells were cultured in 12-well ultralow attachment plates with the concentration of $1 \times 10^5$ cells $ml^{-1}$ for 24 h and incubated with various GNSs nanocomposite particles (40 µg $ml^{-1}$) for another 4 h. The cells were rinsed with PBS thrice and further harvested by centrifugation at 1000 rpm for 5 min. Subsequently the cells were counted and lysed with aqua regia solution. The amount of gold in the cells incubated with various GNSs nanocomposite particles was determined by ICP-OES.

To investigate targeted cellular uptake by FACS, the various GNSs-dPG-IDCC nanocomposite particles were prepared by a reported procedure.[36,45] The mammosphere cells were incubated with various GNSs-dPG-IDCC nanocomposite particles. After being rinsed with PBS three times and harvested by centrifugation, the cells were detected by a flow cytometer (BD FACS Calibur, USA). The internalized cellular accumulation was analyzed by the intensity of IDCC fluorescence.

To investigate the targeted cellular uptake of nanocomposite particles by confocal laser scanning microscope (CLSM), 200 µl mammosphere cells ($2 \times 10^4$ cells per well) were seeded in IBIDI u-Slide 8-well confocal culture ultralow attachment plates for 24 h and incubated with various GNSs-dPG-IDCC nanocomposite particles (40 µg $ml^{-1}$) for another 4 h, respectively. After incubation, the cells were rinsed three times with PBS to remove the free nanocomposite particles, and fixed with 4% paraformaldehyde, permeabilized with 0.2% Triton X-100, and incubated with 1% BSA to block nonspecific binding sites. Finally, the nucleus and cytoskeleton of cells were stained with 4′,6-diamidino-2-phenylindole (DAPI, Life Technologies), and phalloidin-FITC (Abcam), and the fluorescent images were obtained by a CLSM (Leica TCS SP8).

*The HK2 and Mitochondria-Targeted Cellular Uptake Assay*: To evaluate the HK2 targeting ability, the mammosphere cells were incubated with various GNSs-dPG-IDCC nanocomposite particles and treated as described above. Then, the cells were incubated with primary antibody (Anti-Hexokinase II antibody, Abcam) at 4 °C overnight. Afterwards, the cells were rinsed with PBS and stained with fluorochrome-conjugated secondary antibody (Anti-rabbit IgG H+L, Alexa Fluor 488 Conjugate, cell signaling) and subsequently stained the nucleus with DAPI. Then the fluorescent images were obtained by a CLSM.

To evaluate the mitochondria targeting ability, mammosphere cells were incubated with the Cell Light Mitochondria-GFP, BacMam 2.0 in advance for 16 h at 37 °C according to the protocol to label mitochondria. After being incubated with various GNSs-dPG-IDCC nanocomposite particles, the cells were subsequently stained with DAPI and measured by CLSM.

To evaluate the associated bound relationship between HK2 and mitochondria, the mitochondria of mammosphere cells were labeled first, after being fixed, permeabilized. and blocked, the cells were incubated with primary antibody (Anti-Hexokinase II antibody, Abcam) at 4 °C overnight. Then stained with fluorochrome-conjugated secondary antibody (Anti-rabbit IgG H+L, Alexa Fluor 594 conjugate, cell signaling) and DAPI. The fluorescent images were obtained by a CLSM.

*In Vitro Photothermal Therapy Efficacy*: To evaluate the in vitro PTT therapeutic efficacy of CSCs, the mammosphere cells were seeded into 96-well ultralow attachment plates and incubated with PBS, 5–40 µg $ml^{-1}$ of various nanocomposite particles for 4 h. After that, the cells were collected by centrifugation and then the pellets of the cells were irradiated by an 808 nm laser at a power density of 1.5 W $cm^{-2}$ for 5 min. Meanwhile, the temperature value was recorded and corresponding thermal imaging was

**Table 1.** Primer sequences of target genes for qRT-PCR.

| Gene | Forward primers (5'-3') | Reverse primers (5'-3') |
|---|---|---|
| GAPDH | GCAAGAGCACAAGAGGAAGAG | AAGGGGTCTACATGGCAACT |
| SOX2 | GGGAAATGGGAGGGGTGCAAAAGAGG | TTGCGTGAGTGTGGATGGGATTGGTG |
| OCT4 | GACAGGGGGAGGGGAGGAGCTAGG | CTTCCCTCCAACCAGTTGCCCCAAAC |
| NANOG | CAGCCCCGATTCTTCCACCAGTCCC | CGGAAGATTCCCAGTCGGGTTCACC |

taken. After laser irradiation, the cells were re-suspended in fresh medium and cultured in 96-well ultralow attachment plates for another 24 h at 37 °C. Finally, the cellular viability was assessed by CCK8 assay. Furthermore, the viabilities of the mammosphere cells incubated with various nanocomposite particles (40 μg $ml^{-1}$) under the irradiation were also characterized by CAM/EthD-1 staining and then analyzed by using a fluorescence microscope.

*Cytochrome c Immunocytochemical Staining*: To verify the release of cytochrome c after the PTT, the mammosphere cells were seeded in IBIDI u-Slide 8-well confocal culture ultralow attachment plates, then incubated with various nanocomposite particles (40 μg $ml^{-1}$) and treated with PTT. After that, the cells were fixed, permeabilized, and blocked. For the release of cytochrome c staining, the cells were incubated with primary antibody (Cytochrome c Mouse mAb, cell signaling) at 4 °C overnight and then stained with a fluorochrome-conjugated secondary antibody (Anti-mouse IgG H+L, Alexa Fluor 555 Conjugate, cell signaling). After subsequently staining the nucleus with DAPI, the fluorescent images were obtained by a CLSM.

*Determination of $ALDH^+$ Proportion In Vitro*: To evaluate the proportion of CSCs after the PTT, the mammosphere cells were seeded into 12-well ultralow attachment plates followed by incubation with various nanocomposite particles and treated with PTT. The treated cells were harvested and trypsinized. The ALDEFLUOR kit was used to analyze the acetaldehyde dehydrogenase (ALDH) activity of the collected cells. The cells were determined with a BD FACS calibur flow cytometer (Beckton Dickinson).

*Expression of Stemness-Associated Gene*: The mammosphere cells were incubated with various nanocomposite particles and treated with PTT. Further, the RNA of the cells was isolated and pooled via TRI Reagent, and then precipitated in isopropanol and washed with 75% (vol/vol) ethanol/water. The RNA content was quantified by a spectrophotometry (Thermo Fisher; Nano-Drop). One microgram of total RNA was reverse transcribed to cDNA using the SuperScript IV VILO Master Mix (Invitrogen). qRT-PCR was performed with the SYBR Green PCR Master Mix (Thermo Fisher) on the PIKOREAL 96 Real-Time PCR system. Relative mRNA expression levels of SOX2, OCT4, and NANOG were normalized to the housekeeping gene GAPDH using the delta-delta Ct method. Finally, the mRNA levels were normalized to those of the cells treated with irradiation alone. Primer sequences used for qRT-PCR are listed in **Table 1**.

*In Vitro Mammospheres Formation Assay*: For in vitro mammospheres formation assay, the primary mammosphere cells were incubated with various GNSs-dPG nanocomposite particles and treated with or without by PTT as described above. Afterwards, the cells were collected and trypsinized, then 2000 cells were seeded in a new 96-well ultralow attachment plate. After incubation for 10 days in a 5% $CO_2$ incubator at 37 °C, the number of secondary mammospheres (>50 μm) was counted under a microscope and the optical micrographs were also taken.

*In Vivo Biocompatibility*: All the animal experiments and animal care were conducted under the protocols approved by the Regional Ethics Committee for Animal Experiments at Ningbo University (Permit No. SYXK Zhe 2019-0005). For in vivo biocompatibility evaluation of the nanocomposite particles, 12 healthy female Balb/c (nu/nu) nude mice were randomly divided into four groups and intravenously injected by 100 μl of PBS, GNSs-dPG-3BP, GNSs-dPG-3BP, TPP and GNSs-dPG-3BP, TPP, HA at the dose of 10 mg $kg^{-1}$. After one month, the major organs including the heart, liver, spleen, lung, and kidney of the nude mice were harvested and stained with hematoxylin and eosin (H&E) for histological analysis.

*Tumor Model*: Female Balb/c nude mice (14-16 g, 4–5 weeks old) were used to establish the tumor models of 4T1 and MDA-MB-231 in this work. Briefly, the 4T1 cells ($1 \times 10^6$ cells, 100 μl) containing RPMI-1640 were inoculated subcutaneously into the back of each mouse. The MDA-MB-231 cells ($1 \times 10^7$ cells, 100 μl) suspended in a mixture of DMEM and matrigel were inoculated subcutaneously into the back of each mouse. A digital caliper was used to measure the tumor size. The animal experiments were carried out when the tumor reached about 50–100 $mm^3$ (tumor volume = (tumor length) × $(\text{tumor width})^2/2$).

*In Vivo Bio-Distribution*: 4T1 tumor-bearing nude mice were intravenously injected by 100 μL of GNSs-dPG-3BP and 100 μL of GNSs-dPG-3BP, TPP, HA, respectively by using the concentration of 3 mg $ml^{-1}$. After 24 h, the mice were sacrificed, and the main organs (including heart, liver, spleen, lung, kidney, and tumor) were collected and weighted. Further, lysed with aqua regia solution, and heated in a Teflon-lined stainless-steel autoclave. The resulting solutions were diluted with water and the Au amount in each measured organ was determined by ICP-OES.

*In Vivo Photothermal Effect Evaluation*: 4T1 tumor-bearing nude mice were intravenously injected by PBS, GNSs-dPG-3BP, GNSs-dPG-3BP, TPP, and GNSs-dPG-3BP, TPP, HA, respectively. After 24 h, the mice were exposed to the 808 nm laser (1.5 W $cm^{-2}$) for 5 min. The temperature fluctuations in the tumors were recorded and the infrared thermal imaging was taken by using an infrared thermometer.

*In Vivo PTT Therapeutic Effect and CSCs Markers' Expression Staining*: 4T1 tumor-bearing nude mice and MDA-MB-231 tumor-bearing nude mice were intravenously injected with various nanocomposite particles and treated with PTT. 24 h after the irradiation, the tumors were dissected, photographed, and stained with H&E for tumor injury analysis. Furthermore, TUNEL, CD44, SOX2, and NANOG immunohistochemical staining were also performed, and the nuclei were stained using DAPI.

*In Vivo PTT*: For in vivo therapy, 4T1 tumor-bearing nude mice were randomly divided into the following five groups (six mice per group). Injection of PBS with laser irradiation (PBS + L), injection of GNSs-dPG-3BP, TPP, and HA alone (GNSs-dPG-3BP, TPP, and HA), injection of GNSs-dPG-3BP with laser irradiation (GNSs-dPG-3BP + L), injection of GNSs-dPG-3BP, TPP, and HA with laser irradiation (GNSs-dPG-3BP, TPP + L), and injection of GNSs-dPG-3BP, TPP, and HA with laser irradiation (GNSs-dPG-3BP, TPP, HA + L). At 24 h post intravenous (i.v.) injection of 100 μl 3 mg $ml^{-1}$ of various samples, the tumors were irradiated with or without the 808 nm laser (1.5 W $cm^{-2}$) for 5 min. As the treatment started, the tumor volumes and body weights were measured at two days intervals. On the 14th day, the mice were sacrificed, and the main organs (including heart, liver, spleen, lung, and kidney) were dissected for H&E staining.

*Statistical Analysis*: All results are represented as mean ± standard deviation (S.D.) with independent experiments. Statistical analysis of the experimental data was performed using one-way analysis of variance (ANOVA) with the Tukey significant difference post hoc test using Origin 9.0 software. A *p*-value of 0.05 was considered as the level of significance, and the data were classified as (*) for $p < 0.05$, (**) for $p < 0.01$, and (***) for $p < 0.001$.

## Supporting Information

Supporting Information is available from the Wiley Online Library or from the author.

## Acknowledgements

Y.P. gratefully acknowledges financial support from the China Scholarship Council. The authors acknowledge the core facility BioSupraMol, Cathleen Schlesener for dPG-$NH_2$ synthesis, Dr. Christoph Böttcher (Freie Universität Berlin, Germany) for his support with the TEM measurements, and Dr. Pamela Winchester (Freie Universität Berlin, Germany) for language polishing of this manuscript.

Open Access funding enabled and organized by Projekt DEAL.

## Conflict of Interest

The authors declare no conflict of interest.

## Data Availability Statement

The data that support the findings of this study are available in the supplementary material of this article.

## Keywords

breast cancer stem cells, dendritic polyglycerol, gold nanostars, metabolism inhibition, photothermal therapy

Received: October 21, 2021
Revised: December 13, 2021
Published online: January 17, 2022

[1] T. Reya, S. J. Morrison, M. F. Clarke, I. L. Weissman, *Nature* **2001**, *414*, 105.
[2] J. E. Visvader, G. J. Lindeman, *Nat. Rev. Cancer* **2008**, *8*, 755.
[3] B. Beck, C. Blanpain, *Nat. Rev. Cancer* **2013**, *13*, 727.
[4] P. Sancho, D. Barneda, C. Heeschen, *Br. J. Cancer* **2016**, *114*, 1305.
[5] V. Snyder, T. C. Reed-Newman, L. Arnold, S. M. Thomas, S. Anant, *Front. Oncol.* **2018**, *8*, 203.
[6] C. Pecqueur, L. Oliver, K. Oizel, L. Lalier, F. M. Vallette, *Int. J. Cell Biol.* **2013**, *2013*, 805975.
[7] R. A. Cairns, I. S. Harris, T. W. Mak, *Nat. Rev. Cancer* **2011**, *11*, 85.
[8] C. Dong, T. Yuan, Y. Wu, Y. Wang, T. W. Fan, S. Miriyala, Y. Lin, J. Yao, J. Shi, T. Kang, P. Lorkiewicz, D. St Clair, M. C. Hung, B. M. Evers, B. P. Zhou, *Cancer Cell* **2013**, *23*, 316.
[9] D. Ciavardelli, C. Rossi, D. Barcaroli, S. Volpe, A. Consalvo, M. Zucchelli, A. De Cola, E. Scavo, R. Carollo, D. D'Agostino, F. Forli, S. D'Aguanno, M. Todaro, G. Stassi, C. Di Ilio, V. De Laurenzi, A. Urbani, *Cell Death Dis.* **2014**, *5*, e1336.
[10] J. E. Wilson, *J. Exp. Biol.* **2003**, *206*, 2049.
[11] P. L. Pedersen, *J. Bioenerg. Biomembr.* **2008**, *40*, 123.
[12] H. J. Lee, C. F. Li, D. Ruan, J. He, E. D. Montal, S. Lorenz, G. D. Girnun, C. H. Chan, *Nat. Commun.* **2019**, *10*, 2625.
[13] O. Isayev, V. Rausch, N. Bauer, L. Liu, P. Fan, Y. Zhang, J. Gladkich, C. C. Nwaeburu, J. Mattern, M. Mollenhauer, F. Rückert, S. Zach, U. Haberkorn, W. Gross, F. Schönsiegel, A. V. Bazhin, I. Herr, *Oncotarget* **2014**, *5*, 5177.
[14] P. L. Pedersen, *J. Bioenerg. Biomembr.* **2012**, *44*, 1.
[15] Z. Chen, H. Zhang, W. Lu, P. Huang, *Biochim. Biophys. Acta* **2009**, *1787*, 553.
[16] T. Lang, Y. Liu, Z. Zheng, W. Ran, Y. Zhai, Q. Yin, P. Zhang, Y. Li, *Adv. Mater.* **2019**, *31*, 1806202.
[17] S. Shen, J. X. Xia, J. Wang, *Biomaterials* **2016**, *74*, 1.
[18] Z. Zhang, J. Wang, X. Nie, T. Wen, Y. Ji, X. Wu, Y. Zhao, C. Chen, *J. Am. Chem. Soc.* **2014**, *136*, 7317.
[19] H. Li, W. Yan, X. Suo, H. Peng, X. Yang, Z. Li, J. Zhang, D. Liu, *Biomaterials* **2019**, *200*, 1.
[20] Y. Xu, J. Wang, X. Li, Y. Liu, L. Dai, X. Wu, C. Chen, *Biomaterials* **2014**, *35*, 4667.
[21] C. Mei, N. Wang, X. Zhu, K.-H. Wong, T. Chen, *Adv. Funct. Mater.* **2018**, *28*, 1805225.
[22] T. Sun, Y. Wang, Y. Wang, J. Xu, X. Zhao, S. Vangveravong, R. H. Mach, Y. Xia, *Adv. Healthcare Mater.* **2014**, *3*, 1283.
[23] S. Liang, C. Li, C. Zhang, Y. Chen, L. Xu, C. Bao, X. Wang, G. Liu, F. Zhang, D. Cui, *Theranostics* **2015**, *5*, 970.
[24] Y. Pan, X. Ma, C. Liu, J. Xing, S. Zhou, B. Parshad, T. Schwerdtle, W. Li, A. Wu, R. Haag, *ACS Nano* **2021**, *15*, 15069.
[25] Y. Li, R. Zhang, Z. Lu, G. Ma, L. Chen, Q. Tang, X. Zhang, *Small* **2016**, *12*, 5516.
[26] W. Qin, G. Huang, Z. Chen, Y. Zhang, *Front. Pharmacol.* **2017**, *8*, 1.
[27] L. He, J. Gu, L. Y. Lim, Z. X. Yuan, J. Mo, *Front. Pharmacol.* **2016**, *7*, 313.
[28] S. Marrache, S. Dhar, *Chem. Sci.* **2015**, *6*, 1832.
[29] E. B. Kang, I. In, K.-D. Lee, S. Y. Park, *J. Ind. Eng. Chem.* **2017**, *55*, 224.
[30] S. L. Yoong, B. S. Wong, Q. L. Zhou, C. F. Chin, J. Li, T. Venkatesan, H. K. Ho, V. Yu, W. H. Ang, G. Pastorin, *Biomaterials* **2014**, *35*, 748.
[31] T. A. Wang, X. D. Zhang, X. Y. Guo, S. L. Xian, Y. F. Lu, *Oncol. Rep.* **2016**, *35*, 1287.
[32] K. Hu, H. Zhou, Y. Liu, Z. Liu, J. Liu, J. Tang, J. Li, J. Zhang, W. Sheng, Y. Zhao, Y. Wu, C. Chen, *Nanoscale* **2015**, *7*, 8607.
[33] C. Dong, Z. Liu, J. Liu, C. Wu, F. Neumann, H. Wang, M. Schafer-Korting, B. Kleuser, J. Chang, W. Li, N. Ma, R. Haag, *Adv. Healthcare Mater.* **2016**, *5*, 2214.
[34] Z. Tu, H. Qiao, Y. Yan, G. Guday, W. Chen, M. Adeli, R. Haag, *Angew. Chem., Int. Ed. Engl.* **2018**, *57*, 11198.
[35] Y. Zhong, M. Dimde, D. Stobener, F. Meng, C. Deng, Z. Zhong, R. Haag, *ACS Appl. Mater. Interfaces* **2016**, *8*, 27530.
[36] S. Zhou, Y. Pan, J. Zhang, Y. Li, F. Neumann, T. Schwerdtle, W. Li, R. Haag, *Nanoscale* **2020**, *12*, 24006.
[37] J. Vonnemann, N. Beziere, C. Bottcher, S. B. Riese, C. Kuehne, J. Dernedde, K. Licha, C. von Schacky, Y. Kosanke, M. Kimm, R. Meier, V. Ntziachristos, R. Haag, *Theranostics* **2014**, *4*, 629.
[38] M. Calderon, M. A. Quadir, S. K. Sharma, R. Haag, *Adv. Mater.* **2010**, *22*, 190.
[39] H. Yang, Q. Wang, Z. Li, F. Li, D. Wu, M. Fan, A. Zheng, B. Huang, L. Gan, Y. Zhao, X. Yang, *Nano Lett.* **2018**, *18*, 7909.
[40] Y. Pan, S. Zhou, Y. Li, B. Parshad, W. Li, A. Wu, R. Haag, *J. Controlled Release* **2021**, *330*, 1106.
[41] J. Tang, H. Zhou, J. Liu, J. Liu, W. Li, Y. Wang, F. Hu, Q. Huo, J. Li, Y. Liu, C. Chen, *ACS Appl. Mater. Interfaces* **2017**, *9*, 23497.
[42] S. Roller, H. Zhou, R. Haag, *Mol. Diversity* **2005**, *9*, 305.
[43] S. Wang, Y. Tian, W. Tian, J. Sun, S. Zhao, Y. Liu, C. Wang, Y. Tang, X. Ma, Z. Teng, G. Lu, *ACS Nano* **2016**, *10*, 8578.
[44] F. Zabihi, S. Wieczorek, M. Dimde, S. Hedtrich, H. G. Borner, R. Haag, *J. Controlled Release* **2016**, *242*, 35.
[45] D. Groger, F. Paulus, K. Licha, P. Welker, M. Weinhart, C. Holzhausen, L. Mundhenk, A. D. Gruber, U. Abram, R. Haag, *Bioconjugate Chem.* **2013**, *24*, 1507.